

# Analytic characterization of sub-Alfvénic turbulence energetics

R. Skalidis<sup>1\*</sup>, K. Tassis<sup>2,3</sup>, and V. Pavlidou<sup>2,3</sup>

<sup>1</sup> Owens Valley Radio Observatory, California Institute of Technology, MC 249-17, Pasadena, CA 91125, USA

<sup>2</sup> Department of Physics & ITCP, University of Crete, GR-70013, Heraklion, Greece

<sup>3</sup> Institute of Astrophysics, Foundation for Research and Technology-Hellas, Vasilika Vouton, GR-70013 Heraklion, Greece

## ABSTRACT

Magnetohydrodynamic (MHD) turbulence is a cross-field process relevant to many systems. A prerequisite for understanding these systems is to constrain the role of MHD turbulence, and in particular, the energy exchange between kinetic and magnetic forms. The energetics of strongly magnetized and compressible turbulence has so far resisted attempts to understand them. Numerical simulations reveal that kinetic energy can be orders of magnitude higher than fluctuating magnetic energy. We solved this lack-of-balance puzzle by calculating the energetics of compressible and sub-Alfvénic turbulence based on the dynamics of coherent cylindrical fluid parcels. Using the MHD Lagrangian, we proved analytically that the bulk of the magnetic energy transferred to kinetic energy is the energy that is stored in the coupling between the ordered and fluctuating magnetic field. The analytical relations are in strikingly good agreement with numerical data, up to second-order terms.

## 1. Introduction

Magnetohydrodynamic (MHD) turbulence is involved in a plethora of physical phenomena (Biskamp 2003; Beresnyak 2019; Matthaeus & Velli 2011; Matthaeus 2021; Schekochihin 2020). The interplay between kinetic and magnetic energy is important for understanding these processes (Goldstein et al. 1995; Ciolek & Basu 2006; Kirk et al. 2009; Oughton et al. 2013; Matthaeus et al. 1983; Zweibel & McKee 1995; Schekochihin et al. 2007; Cho & Lazarian 2002; Federrath et al. 2011). It is challenging to understand the energy exchange between kinetic and magnetic forms because the MHD equations are nonlinear. For this reason, several assumptions and approximations are usually employed.

A widely employed approximation is the incompressibility of the gas (Sridhar & Goldreich 1994; Goldreich & Sridhar 1995), although this is only applicable to a limited number of systems. Compressible MHD turbulence is more complex, and additional energy terms contribute to the energy cascade. One main difference in the energy cascade rate of incompressible and compressible turbulence is that in the latter, the background magnetic field ( $\mathbf{B}_0$ ) appears with leading-order terms (Banerjee & Galtier 2013; Andrés & Sahaoui 2017). In contrast, the incompressible turbulence energy cascade is dominated by the increments of the magnetic and velocity fluctuations, and  $\mathbf{B}_0$  only appears in higher-order statistics (Wan et al. 2012). This result motivated the hypothesis that  $\mathbf{B}_0$  might also appear in the total (kinetic and magnetic) fluctuating energy of compressible MHD turbulence (Andrés & Sahaoui 2017), whereas in incompressible turbulence, the total fluctuating energy is dominated by the fluctuating (second-order) kinetic and magnetic energy.

In incompressible and sub-Alfvénic turbulence, the fluctuating magnetic energy is completely transferred to kinetic energy, and the volume-averaged quantities are in equilibrium,  $\rho\langle u^2 \rangle / 2 \sim \langle \delta B^2 \rangle / 8\pi$ , when turbulence is maintained in a steady state. In contrast, direct numerical simulations of sub-Alfvénic and compressible turbulence show that the volume-averaged kinetic energy is much higher than the second-order fluctuating

magnetic energy,  $\rho\langle u^2 \rangle / 2 \gg \langle \delta B^2 \rangle / 8\pi$  (Heitsch et al. 2001; Li et al. 2012a,b), and their relative ratio depends on the amplitude of  $\mathbf{B}_0$  (Andrés et al. 2018; Lim et al. 2020; Skalidis et al. 2021; Beattie et al. 2022b). The excess of the kinetic energy suggests that  $\mathbf{B}_0$  might provide additional energy to the fluid.

The role of  $\mathbf{B}_0$  in the energetics can be intuitively understood when we decompose the total magnetic field into a background and a fluctuating component. In incompressible turbulence, the fluctuating magnetic energy comes only from the perturbations of the magnetic field, which are of second order. However, in compressible turbulence, the background field appears in the total fluctuating magnetic energy due to the coupling between the background field and magnetic perturbations ( $\delta\mathbf{B}$ ). The magnetic coupling, expressed as  $\mathbf{B}_0 \cdot \delta\mathbf{B}$ , can only be realized in compressible turbulence (Montgomery et al. 1987; Bhattacharjee & Hameiri 1988; Bhattacharjee et al. 1998; Fujimura & Tsuneta 2009) and is the dominant (first-order) term of the fluctuating magnetic energy.

In sub-Alfvénic and compressible turbulence, numerical data show that  $\mathbf{B}_0 \cdot \delta\mathbf{B}$  stores most of the magnetic energy, and that the kinetic energy approximately reaches equipartition with the fluctuations of the coupling term (Skalidis & Tassis 2021; Skalidis et al. 2021; Beattie et al. 2022b,a). Thus, the magnetic coupling holds the key for understanding the energetics of strongly magnetized and compressible turbulence. However, there is still a lack of first-principle understanding of the role of  $\mathbf{B}_0 \cdot \delta\mathbf{B}$  in MHD turbulence dynamics and how it contributes to the averaged energetics.

We present an analytical theory of the role of the coupling potential in the energy exchange of sub-Alfvénic and compressible turbulence, which is encountered in systems such as tokamaks (Strauss 1976, 1977; Zocco & Schekochihin 2011), in the interstellar medium (Mouschovias et al. 2006; Panopoulou et al. 2015, 2016; Planck Collaboration et al. 2016; Skalidis et al. 2022), and the Sun (Verdini & Velli 2007; Tenerani & Velli 2017; Kasper et al. 2021; Zank et al. 2022). We write the Lagrangian of coherent flux structures (Crowley et al. 2022), which allows us to approximate turbulence properties in a deterministic manner, and calculate analytically the energy exchange between kinetic

\* skalidis@caltech.edu

and magnetic forms as a function of the Alfvénic Mach number ( $\mathcal{M}_A$ ). We find remarkable agreement between the analytically calculated energetics and numerical data. We conclude that the majority of the fluctuating magnetic energy transferred to kinetic energy is provided by the coupling between the background and the fluctuating magnetic field.

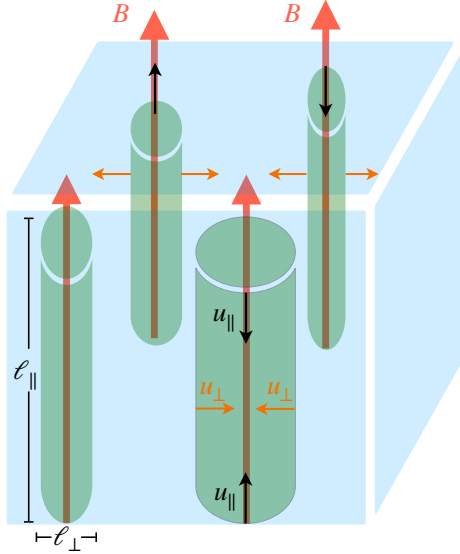


**Fig. 1.** Magnetized fluid consisting of multiple coherent cylindrical fluid parcels. Red arrows show the initial magnetic field morphology. Untwisted fluid parcels are elongated,  $\ell_{\parallel} \gg \ell_{\perp}$ , and their motion is longitudinal along or perpendicular to  $\mathbf{B}_0$ . In sub-Alfvénic turbulence, the motion of these fluid parcels can be decomposed into two independent velocity components, parallel (black arrows) and perpendicular (orange arrows) to  $\mathbf{B}_0$ .

## 2. Model

We considered a turbulent fluid characterized by the commonly employed properties: 1) spatial homogeneity, 2) infinite magnetic and kinetic Reynolds number, and 3) time stationarity. We considered that the fluid consists of coherent flux tubes (e.g., Fig. 1 in Banerjee & Galtier 2013) (or fluid parcels) with coordinates  $(r(t), \phi(t), z(t))$ , as shown in Fig. 1. Cylindrical coordinates are motivated by studies showing that the properties of strongly magnetized turbulence are axially symmetric, with  $\mathbf{B}_0$  being the axis of symmetry (Goldreich & Sridhar 1995; Maron & Goldreich 2001). We assumed the following initial conditions: 1) uniform temperature, 2) uniform density, 3) no bulk velocity, 4) uniform static magnetic field ( $\mathbf{B}_0 = B_0 \hat{z}$ ), and 5) no self-gravity. We henceforth adopt the following notation:  $z = \ell_{\parallel}$  and  $r = \ell_{\perp}$ , where  $\ell_{\parallel}$  and  $\ell_{\perp}$  denote parcel sizes parallel and perpendicular to  $\mathbf{B}_0$ , respectively.

We perturbed the magnetic field of a coherent fluid structure with a length scale  $\ell = \sqrt{\ell_{\parallel}^2 + \ell_{\perp}^2}$  by  $\delta \mathbf{B}_{\ell}$  such that  $|\mathbf{B}_0| \gg |\delta \mathbf{B}_{\ell}|$ , which applies to sub-Alfvénic turbulence. Magnetic perturbations tend to redistribute the magnetic flux within a fluid. For ideal-MHD (flux-freezing) conditions, the magnetic flux is preserved. Thus, the surface of the perturbed fluid parcel ( $\mathcal{S}_{\ell}$ ) follows the magnetic field lines. The motion of the field lines, and hence of  $\mathcal{S}_{\ell}$ , can be either parallel or perpendicular to  $\mathbf{B}_0$  (Fig. 1): 1) Squeezing and stretching of  $\mathcal{S}_{\ell}$  along  $\mathbf{B}_0$  leads to parallel motions,  $\dot{\ell}_{\parallel} \neq 0$ . 2) Fluctuations of  $\ell_{\perp}$  lead to perpendicular motions,  $\dot{\ell}_{\perp} \neq 0$ . Finally, 3) twisting leads to rotational motions,  $\dot{\phi} \neq 0$ .

This naturally defines  $\ell_{\parallel}$  and  $\ell_{\perp}$  as the coherence lengths of the perturbed volume parallel and perpendicular to  $\mathbf{B}_0$ , respectively. We focused on large scales since coherent structures are prominent there (De Giorgio et al. 2017). We invoke as a boundary condition a local freezing environment beyond  $\ell$  (pressure wall).

The flux freezing theorem is

$$\frac{d\mathbf{B}_{\ell}}{dt} \cdot \mathcal{S}_{\ell} = -\mathbf{B}_{\ell} \cdot \frac{d\mathcal{S}_{\ell}}{dt}. \quad (1)$$

The cross section of the coherent volume perpendicular and parallel to  $\mathbf{B}_0$  is  $\mathcal{S}_{\perp, \ell} = 2\pi \ell_{\perp} \ell_{\parallel} \hat{r}$ , and  $\mathcal{S}_{\parallel, \ell} = \pi \ell_{\perp}^2 \hat{z}$ , respectively. The cross section related to the rotational motion is  $\mathcal{S}_{\phi, \ell} = \ell_{\parallel} \ell_{\perp} \hat{\phi}$ . The total magnetic field in cylindrical coordinates can be expressed as  $\mathbf{B}_{\ell} = \delta B_{\perp, r, \ell} \hat{r} + \delta B_{\perp, \phi, \ell} \hat{\phi} + (B_0 + \delta B_{\parallel, \ell}) \hat{z}$ . From Eq. 1, we obtain that when  $|\mathbf{B}_0| \gg |\delta \mathbf{B}|$ , magnetic perturbations along  $\mathcal{S}_{\parallel, \ell}$  are associated with a longitudinal motion such that

$$u_{\perp, r, \ell} \equiv \dot{\ell}_{\perp}(t) = -\frac{\delta \dot{B}_{\parallel, \ell}(t)}{2B_0 + \delta B_{\parallel, \ell}} \ell_{\perp}(t) \approx -\frac{\delta \dot{B}_{\parallel, \ell}(t)}{2B_0} \ell_{\perp, 0}, \quad (2)$$

where we have considered that the initial dimension of the perturbed volume  $\ell_{\perp, 0}$  is much larger than its perturbations. Along  $\mathcal{S}_{\perp, \ell}$ , we find that

$$u_{\parallel, \ell} \equiv \dot{\ell}_{\parallel}(t) = -\left( \frac{\delta \dot{B}_{\perp, r, \ell}(t)}{\delta B_{\perp, r, \ell}(t)} - \frac{\delta \dot{B}_{\parallel, \ell}(t)}{2B_0} \right) \ell_{\parallel}(t) \approx -\frac{\delta \dot{B}_{\perp, r, \ell}(t)}{\delta B_{\perp, r, \ell}(t)} \ell_{\parallel}(t), \quad (3)$$

while the azimuthal velocity along  $\mathcal{S}_{\phi, \ell}$  is

$$u_{\perp, \phi, \ell} \equiv \dot{\phi}(t) \ell_{\perp}(t) \approx -\left( \frac{\delta \dot{B}_{\perp, r, \ell}(t)}{\delta B_{\perp, r, \ell}(t)} - \frac{\delta \dot{B}_{\perp, \phi, \ell}(t)}{\delta B_{\perp, \phi, \ell}(t)} \right) \ell_{\perp}(t). \quad (4)$$

As a result of assuming  $|\mathbf{B}_0| \gg |\delta \mathbf{B}|$ , we have obtained that parallel and perpendicular motions are decoupled. The coupling of parallel and perpendicular motions becomes inevitable when  $|\mathbf{B}_0| \sim |\delta \mathbf{B}|$  (Eq. 3).

In sub-Alfvénic turbulence, magnetic tension dominates magnetic pressure (Passot & Vázquez-Semadeni 2003). The high tension suppresses transverse oscillations due to the strong restoring torques. Thus, twisting would have minimum contribution to the dynamics (e.g., Longcope & Klapper 1997) and motions would be mostly longitudinal ( $\dot{\phi}, \delta B_{\perp, \phi, \ell} \approx 0$ ). Since  $u_{\perp, \phi, \ell} \rightarrow 0$ , then due to Eqs. 3, and 4,  $\ell_{\parallel} \gg \ell_{\perp}$ , which implies that untwisted coherent structures are stretched toward the  $\mathbf{B}_0$  axis, which is consistent with the anisotropic properties of sub-Alfvénic turbulence (Shebalin et al. 1983; Higdon 1984; Oughton et al. 1994; Sridhar & Goldreich 1994; Goldreich & Sridhar 1995; Oughton et al. 2013; Oughton & Matthaeus 2020; Cho & Lazarian 2003; Yang et al. 2018; Makwana & Yan 2020; Gan et al. 2022).

For untwisted fluid parcels, the perpendicular component of the magnetic fluctuations has a dominant radial component such that  $\delta B_{\perp, \ell} \approx \delta B_{\perp, r, \ell}$ . From Eqs. 2 and 3, we derive

$$\delta B_{\parallel, \ell}(t) \propto -B_0 \log \ell_{\perp}(t), \quad (5)$$

$$\delta B_{\perp, \ell}(t) \propto \ell_{\parallel}^{-1}(t). \quad (6)$$

The difference in the scaling is due to the Lorenz force by  $\mathbf{B}_0$ , which affects perpendicular motions, while it has no effect on parallel motions.

### 3. MHD Lagrangian of coherent structures

We write the Lagrangian for the perturbed volume. We place the reference frame at the center of mass of the target volume, hence there is no bulk velocity term in the Lagrangian. Therefore, all the velocity components are due to internal motions induced by magnetic perturbations. We focus on low plasma-beta fluids<sup>1</sup>, which for sub-Alfvénic turbulence corresponds to high sonic Mach numbers ( $\mathcal{M}_s$ ). The perturbed Lagrangian (Newcomb 1962; Andreussi et al. 2016; Kulsrud 2005) of the coherent cylindrical fluid parcel, with surface  $\mathcal{S}_\ell$ , can be split into a parallel and a perpendicular term (Appendix A),

$$\delta\mathcal{L} = \overbrace{\left( \frac{1}{2}\rho\dot{\ell}_\perp^2 - \frac{\delta B_{\perp,\ell}^2}{8\pi} \right)}^{\delta\mathcal{L}_\perp} + \overbrace{\left( \frac{1}{2}\rho\dot{\ell}_\parallel^2 - \frac{B_0\delta B_{\parallel,\ell}}{4\pi} - \frac{\delta B_{\parallel,\ell}^2}{8\pi} \right)}^{\delta\mathcal{L}_\parallel}. \quad (7)$$

Due to Eqs. 2 and 3,  $\delta B_{\parallel,\ell}$ , and  $\delta B_{\perp,\ell}$  are generalized coordinates of  $\delta\mathcal{L}$  and  $\ell_\parallel(t) = C/\delta B_{\perp,\ell}(t)$  (Eq. 6), where  $C$  is a constant determined from the initial conditions. With this expression, we eliminate  $\ell_\parallel$  from the Lagrangian, which up to second-order terms is separable into a parallel and a perpendicular part, and is analytically solvable,

$$\delta\mathcal{L}_\perp(\delta B_{\perp,\ell}, \delta\dot{B}_{\perp,\ell}) \approx \frac{1}{2}\rho C^2 \frac{\delta\dot{B}_{\perp,\ell}^2}{\delta B_{\perp,\ell}^4} - \frac{\delta B_{\perp,\ell}^2}{8\pi}, \quad (8)$$

$$\delta\mathcal{L}_\parallel(\delta B_{\parallel,\ell}, \delta\dot{B}_{\parallel,\ell}) \approx \frac{1}{8}\rho \frac{\delta\dot{B}_{\parallel,\ell}^2}{B_0^2} \ell_{\perp,0}^2 - \frac{B_0\delta B_{\parallel,\ell}}{4\pi} - \frac{\delta B_{\parallel,\ell}^2}{8\pi}. \quad (9)$$

We solve the Euler-Lagrange equations for  $\delta\mathcal{L}_\parallel$  (Appendix B) and  $\delta\mathcal{L}_\perp$  (Appendix C) and derive the analytical solutions of the velocity ( $u_{\parallel,\ell}(t)$ ,  $u_{\perp,\ell}(t)$ ) and magnetic fluctuations ( $\delta B_{\parallel,\ell}(t)$ ,  $\delta B_{\perp,\ell}(t)$ ) of  $\mathcal{S}_\ell$ . We find that  $\delta B_{\parallel,\ell} \sim t^2$ ,  $u_{\perp,\ell} \sim t$ , and  $\delta B_{\perp,\ell} \sim t^{-1}$ , while  $u_{\parallel,\ell}$  is set by the initial conditions (**free streaming of the gas**). We used these analytical solutions in order to calculate the averaged energetics of a strongly magnetized and compressible fluid.

### 4. Energetics

The total energy of fully developed turbulence is stationary because energy diffusion is balanced by injection. Time stationarity enables us to approximate turbulence energetics with the leading-order solutions that we obtained because our approximations preserve time symmetry, and thus energy is conserved. The statistical properties of large-scale coherent structures accurately approximate the volume-averaged turbulent statistical properties. Thus, for an ergodic fluid (Monin & I'Agglom 1971; Galanti & Tsinober 2004), averaging the turbulent statistical properties over the volume of the fluid at a given time step ( $\langle f \rangle_V = \int_V f$ ) is approximately equivalent to averaging over multiple realizations of a typical large-scale coherent structure ( $\langle f \rangle_{\mathcal{T}} = \int_{\mathcal{T}} f$ ), hence  $\langle f \rangle_V \sim \langle f \rangle_{\mathcal{T}}$ , where  $f$  denotes an energy term, and  $\mathcal{T}$  corresponds to the coherent structure crossing time. We next analytically compute the  $\langle f \rangle_{\mathcal{T}}$  energy contribution of each Lagrangian term (Eq. 7) and their relative ratios. Since coherent cylindrical parcels are characterized by two different coherence lengths  $\ell_\parallel$  and  $\ell_\perp$ , they also have two different crossing times:  $\mathcal{T}_\parallel$  and  $\mathcal{T}_\perp$ , respectively. We compare the  $\langle f \rangle_{\mathcal{T}}$  analytical energy ratios with

<sup>1</sup> The relative ratio of the thermal and magnetic pressure is the plasma beta, which is defined as  $\beta = 2\mathcal{M}_A^2/\mathcal{M}_S^2$ .

the  $\langle f \rangle_V$  numerical values. The numerical results correspond to simulations of ideal isothermal MHD turbulence without self-gravity, and turbulence is maintained in a quasi-static state by injecting energy with an external forcing mechanism (Beattie et al. 2022b). These simulation are forced with a mixture of compressible and incompressible modes, but the driving modes do not affect the energetics of sub-Alfvénic and compressible turbulence (Skalidis et al. 2021).

#### 4.1. Kinetic energy

The total averaged kinetic energy ( $E_{\text{kinetic}}$ ) of the coherent fluid parcel with scale  $\ell$  is

$$E_{\text{kinetic}} \equiv \frac{1}{2}\rho\langle u_\ell^2 \rangle_{\mathcal{T}} = \frac{1}{2}\rho(\langle u_{\perp,\ell}^2 \rangle_{\mathcal{T}_\perp} + \langle u_{\parallel,\ell}^2 \rangle_{\mathcal{T}_\parallel}) \approx \frac{B_0\delta B_{\parallel,\text{max}}}{6\pi} + \frac{\delta B_{\perp,\text{max}}^2}{8\pi}. \quad (10)$$

The kinetic energy is dominated to first order by  $u_{\perp,\ell}$ . Thus, the average Alfvénic Mach number to first order is

$$\mathcal{M}_{\mathcal{A}} \equiv \frac{\sqrt{\langle u_\ell^2 \rangle_{\mathcal{T}}}}{V_A} \approx \sqrt{\frac{4\delta B_{\parallel,\text{max}}}{3B_0}}. \quad (11)$$

#### 4.2. Harmonic potential

From Eqs. B.3 and C.2, we find that  $\langle \delta B_{\parallel,\ell}^2 \rangle_{\mathcal{T}_\perp} = 7\delta B_{\parallel,\text{max}}^2/15$ , and  $\langle \delta B_{\perp,\ell}^2 \rangle_{\mathcal{T}_\parallel} = \delta B_{\perp,\text{max}}^2/2$ . The total time-averaged harmonic potential energy ( $E_{\text{harmonic}}$ ) density is equal to

$$E_{\text{harmonic}} \equiv \frac{\langle \delta B_\ell^2 \rangle_{\mathcal{T}}}{8\pi} \approx \frac{\delta B_{\parallel,\text{max}}^2}{8\pi} \left( \frac{7}{15} + \frac{\zeta^2(\mathcal{M}_A)}{2} \right), \quad (12)$$

where  $\zeta = \delta B_{\perp,\text{max}}/\delta B_{\parallel,\text{max}}$ . Sub-Alfvénic turbulence is anisotropic (Shebalin et al. 1983; Higdon 1984; Oughton et al. 1994; Goldreich & Sridhar 1995), with the anisotropy between  $\delta B_\perp$  and  $\delta B_\parallel$  depending on  $\mathcal{M}_{\mathcal{A}}$  (Beattie et al. 2020). To account for this property, we assumed that  $\zeta$  is a function of  $\mathcal{M}_{\mathcal{A}}$ . When  $\mathcal{M}_{\mathcal{A}} \rightarrow 0$ ,  $B_0$  suppresses any bending of the magnetic field lines with the amplitude of  $\delta B_\parallel$  being larger than that of  $\delta B_\perp$  (Beattie et al. 2020), hence  $\zeta \rightarrow 0$ ; this is also a consequence of  $\nabla \cdot \mathbf{B} = 0$  for anisotropic fluid parcels with  $\ell_\parallel \gg \ell_\perp$ . For  $\mathcal{M}_{\mathcal{A}} \rightarrow 1$ , fluctuations tend to become more isotropic, and hence  $\zeta \rightarrow \sqrt{2}$ . These limiting behaviors are consistent with numerical simulations (Beattie et al. 2020, 2022b).

#### 4.3. Coupling potential

According to Eq. 10,  $\mathbf{B}_0 \cdot \delta\mathbf{B}$  contributes to  $E_{\text{kinetic}}$  since

$$E_{\text{coupling}} \equiv \frac{B_0 \sqrt{\langle \delta B_{\parallel,\ell}^2 \rangle_{\mathcal{T}_\perp}}}{4\pi} \approx \frac{B_0\delta B_{\parallel,\text{max}}}{6\pi} \approx E_{\text{kinetic}}, \quad (13)$$

to first order. This equation demonstrates that the energy stored in the coupling potential is in equipartition with the averaged kinetic energy when turbulence is sub-Alfvénic.

#### 4.4. Energetics ratios

The  $E_{\text{kinetic}}/E_{\text{coupling}}$  ratio is

$$\frac{E_{\text{kinetic}}}{E_{\text{coupling}}} \approx 1 + \frac{9}{16}\mathcal{M}_A^2\zeta^2(\mathcal{M}_{\mathcal{A}}). \quad (14)$$

For  $\mathcal{M}_{\mathcal{A}} \rightarrow 0$ ,  $E_{\text{coupling}} \approx E_{\text{kinetic}}$ , while for  $\mathcal{M}_{\mathcal{A}} \rightarrow 1$ ,  $E_{\text{kinetic}} \gtrsim E_{\text{coupling}}$ .  $E_{\text{kinetic}}$  becomes higher than  $E_{\text{coupling}}$  because  $u_{\parallel,\ell}$  contributes more to  $E_{\text{kinetic}}$  as  $\mathcal{M}_{\mathcal{A}}$  increases. When  $\mathcal{M}_{\mathcal{A}} \rightarrow 1$ ,  $\zeta \approx \sqrt{2}$ , so that the  $E_{\text{kinetic}}/E_{\text{coupling}}$  ratio in trans-Alfvénic turbulence scales as

$$\frac{E_{\text{kinetic}}}{E_{\text{coupling}}} \approx 1 + \frac{9}{8} \mathcal{M}_{\mathcal{A}}^2. \quad (15)$$

Regarding the  $E_{\text{harmonic}}/E_{\text{coupling}}$  ratio, we find that

$$\frac{E_{\text{harmonic}}}{E_{\text{coupling}}} \approx \frac{3}{8} \sqrt{\frac{15}{7}} \mathcal{M}_{\mathcal{A}}^2 \left( \frac{7}{15} + \frac{\zeta^2(\mathcal{M}_{\mathcal{A}})}{2} \right), \quad (16)$$

which for the two limiting cases of  $\zeta$  ( $\mathcal{M}_{\mathcal{A}}$ ) becomes

$$\frac{E_{\text{harmonic}}}{E_{\text{coupling}}} \approx \begin{cases} 0.25 \mathcal{M}_{\mathcal{A}}^2, & \mathcal{M}_{\mathcal{A}} \rightarrow 0 \\ 0.80 \mathcal{M}_{\mathcal{A}}^2, & \mathcal{M}_{\mathcal{A}} \rightarrow 1 \end{cases}. \quad (17)$$

#### 4.5. Comparison between analytical and numerical results

In Fig. 2 we compare the analytically calculated energy ratios with numerical results from the literature (Beattie et al. 2022b). The lines correspond to the analytical relations for  $E_{\text{harmonic}}/E_{\text{coupling}}$  (Eq. 17) and  $E_{\text{kinetic}}/E_{\text{harmonic}}$  (Eq. 15), while the colored points correspond to the numerical values. The numerical data behave as predicted by the analytical relations. The scatter of triangles increases at higher  $\mathcal{M}_{\mathcal{A}}$  because thermal pressure starts becoming important there, and hence the contribution of thermal motions to the kinetic energy increases. In the limit of  $\mathcal{M}_{\mathcal{A}} \ll 1$ , thermal pressure is subdominant and  $\beta \rightarrow 0$ . For  $\mathcal{M}_{\mathcal{A}} = 1$ , we obtain that  $\beta \rightarrow 0$  when  $\mathcal{M}_s \gg 1$ , while when  $\mathcal{M}_s \lesssim 1$ ,  $\beta \rightarrow 1$ . Thus, for trans-Alfvénic turbulence, thermal pressure becomes important only for low  $\mathcal{M}_s$ , while at high  $\mathcal{M}_s$ , it has a minor contribution to the energetics. In our calculations, we neglected thermal pressure, and for this reason, at  $\mathcal{M}_{\mathcal{A}} = 1$ , triangles are consistent with the analytical ratio of  $E_{\text{kinetic}}/E_{\text{coupling}}$  (blue line) when  $\mathcal{M}_s \geq 2$ , while at lower  $\mathcal{M}_s$ , the deviation between numerical and analytical results increases because  $\beta$ , hence the relative contribution of thermal pressure, increases. For  $\mathcal{M}_{\mathcal{A}} < 1$ ,  $\beta \ll 1$ , and for this reason, the numerical data agree perfectly with the analytical ratio (blue line). Finally, when we account for the contribution from both  $\mathbf{B}_0 \cdot \delta \mathbf{B}$  and  $\delta B^2$ , the total energy stored in magnetic fluctuations ( $E_{\text{m,total}} = E_{\text{coupling}} + E_{\text{harmonic}}$ ) is very close to equipartition with kinetic energy, as shown by the red boxes.

## 5. Discussion and conclusions

Analytical calculations of strongly magnetized and compressible (isothermal) turbulence show that  $\mathbf{B}_0$  appears in the energy cascade with leading-order terms (Banerjee & Galtier 2013; Andrés et al. 2018). This is in striking contrast to incompressible turbulence, where  $\mathbf{B}_0$  appears in higher-order terms (Wan et al. 2012). In the formalism presented here, the incompressible limit is approximated when  $\mathbf{B}_0 \cdot \delta \mathbf{B} = 0$ . In this case,  $\mathbf{B}_0$  does not appear in the dominant Lagrangian terms, hence the averaged kinetic energy would scale linearly with the fluctuating magnetic energy,  $\delta u_{\ell} \sim \delta B_{\ell}$  (or equivalently,  $\mathcal{M}_{\mathcal{A}} \sim \delta B_{\ell}$ ). However, in agreement with previous works (Wan et al. 2012), our formalism shows that  $\mathbf{B}_0$  appears in the energetics of incompressible turbulence because of the coupling between  $\delta B_{\parallel,\ell}$  and  $\delta B_{\perp,\ell}$  (Eqs. 3) when higher-order terms are considered.

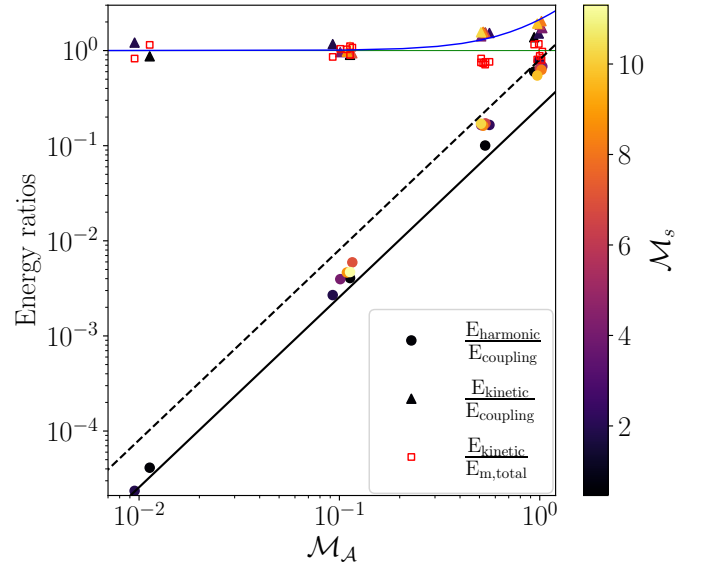


**Fig. 2.** Comparison between analytical and numerical results. The solid and dashed thick black lines correspond to the  $E_{\text{harmonic}}/E_{\text{coupling}}$  ratio obtained analytically for  $\mathcal{M}_{\mathcal{A}} \rightarrow 0$  ( $\zeta = 0$ ) and  $\mathcal{M}_{\mathcal{A}} \rightarrow 1$  ( $\zeta = \sqrt{2}$ ), respectively. Numerical data are shown with colored dots. The blue line corresponds to the analytically obtained  $E_{\text{kinetic}}/E_{\text{coupling}}$  ratio, while colored triangles show the same quantities calculated from numerical data. The red boxes correspond to  $E_{\text{kinetic}}/E_{\text{m,total}}$ . The thin green line shows the energy terms in equipartition. The color bar shows the sonic Mach number ( $\mathcal{M}_s$ ) of the simulations.

For sub-Alfvénic and compressible turbulence, we find that  $\mathbf{B}_0 \cdot \delta \mathbf{B}$  is the leading term in the dynamics, and as a result, the scaling between velocity and magnetic fluctuations becomes  $\delta u_{\ell} \sim \sqrt{B_0 \delta B_{\ell}}$ , or equivalently,  $\mathcal{M}_{\mathcal{A}} \sim \delta u_{\ell}/V_A \sim \sqrt{\delta B_{\ell}/B_0}$ , which is supported by numerical data (Beattie et al. 2020). In compressible and strongly magnetized turbulence, compression and dilatation of the gas locally changes the energy cascade rate (Banerjee & Galtier 2013). These local energy fluctuations can only be realized in compressible turbulence and might be related to the fluctuations of the  $\mathbf{B}_0 \cdot \delta \mathbf{B}$  potential. Our analytical results prove that the total averaged magnetic energy transferred to kinetic is equal to  $(2B_0 \sqrt{\langle \delta B_{\parallel}^2 \rangle} + \langle \delta B^2 \rangle)/8\pi$ .

The consistency between our analytical relations and numerical data is remarkable. It is not the first time that simple analytical arguments agree quantitatively with numerical simulations of nonlinear problems (e.g., Mouschovias et al. 2011). However, an analytical theory is always advantageous because it allows us to achieve a deeper understanding of complex problems. For this reason, the formalism we presented might offer new insights into the energetics of strongly magnetized and compressible turbulence. We hope that it motivates future works about the role of magnetic couplings in the energy cascade.

## References

- Andrés, N. & Sraoui, F. 2017, Phys. Rev. E, 96, 053205  
Andrés, N., Sraoui, F., Galtier, S., et al. 2018, Journal of Plasma Physics, 84, 905840404  
Andreussi, T., Morrison, P. J., & Pegoraro, F. 2016, Physics of Plasmas, 23, 102112  
Banerjee, S. & Galtier, S. 2013, Phys. Rev. E, 87, 013019  
Basu, S., Ciolek, G. E., Dapp, W. B., & Wurster, J. 2009, New A, 14, 483  
Beattie, J. R., Federrath, C., & Seta, A. 2020, MNRAS, 498, 1593  
Beattie, J. R., Krumholz, M. R., Federrath, C., Sampson, M., & Crocker, R. M. 2022a, arXiv e-prints, arXiv:2203.13952

- Beattie, J. R., Krumholz, M. R., Skalidis, R., et al. 2022b, arXiv e-prints, arXiv:2202.13020
- Beresnyak, A. 2019, *Living Reviews in Computational Astrophysics*, 5, 2
- Bhattacharjee, A. & Hameiri, E. 1988, *Physics of Fluids*, 31, 1153
- Bhattacharjee, A., Ng, C. S., & Spangler, S. R. 1998, *ApJ*, 494, 409
- Biskamp, D. 2003, *Plasma Physics and Controlled Fusion*, 45, 1827
- Cho, H., Ryu, D., & Kang, H. 2022, *ApJ*, 926, 183
- Cho, J. & Lazarian, A. 2002, *Phys. Rev. Lett.*, 88, 245001
- Cho, J. & Lazarian, A. 2003, *MNRAS*, 345, 325
- Ciolek, G. E. & Basu, S. 2006, *ApJ*, 652, 442
- Colman, T., Robitaille, J.-F., Hennebelle, P., et al. 2022, *MNRAS*, 514, 3670
- Crowley, C. J., Pughe-Sanford, J. L., Toler, W., et al. 2022, *Proceedings of the National Academy of Science*, 119, e2120665119
- De Giorgio, E., Servidio, S., & Veltri, P. 2017, *Scientific Reports*, 7, 13849
- Elmegreen, B. G. 2009, in *The Galaxy Disk in Cosmological Context*, ed. J. Andersen, Nordströara, B. m, & J. Bland-Hawthorn, Vol. 254, 289–300
- Elmegreen, B. G. & Scalo, J. 2004, *ARA&A*, 42, 211
- Eswaran, V. & Pope, S. B. 1988, *Computers and Fluids*, 16, 257
- Federrath, C., Chabrier, G., Schober, J., et al. 2011, *Phys. Rev. Lett.*, 107, 114504
- Fujimura, D. & Tsuneta, S. 2009, *ApJ*, 702, 1443
- Galanti, B. & Tsinober, A. 2004, *Physics Letters A*, 330, 173
- Gan, Z., Li, H., Fu, X., & Du, S. 2022, *ApJ*, 926, 222
- Girichidis, P., Walch, S., Naab, T., et al. 2016, *MNRAS*, 456, 3432
- Goldreich, P. & Sridhar, S. 1995, *ApJ*, 438, 763
- Goldstein, M. L., Roberts, D. A., & Matthaeus, W. H. 1995, *Annual Review of Astronomy and Astrophysics*, 33, 283
- Hanasoge, S. M., Hotta, H., & Sreenivasan, K. R. 2020, *Science Advances*, 6, eaba9639
- Heitsch, F., Zweibel, E. G., Mac Low, M.-M., Li, P., & Norman, M. L. 2001, *ApJ*, 561, 800
- Higdon, J. C. 1984, *ApJ*, 285, 109
- Iffrig, Olivier & Hennebelle, Patrick. 2017, *A&A*, 604, A70
- Kasper, J. C., Klein, K. G., Lichko, E., et al. 2021, *Phys. Rev. Lett.*, 127, 255101
- Kirk, H., Johnstone, D., & Basu, S. 2009, *ApJ*, 699, 1433
- Klessen, R. S. & Hennebelle, P. 2010, *A&A*, 520, A17
- Kritsuk, A. G., Ustyugov, S. D., & Norman, M. L. 2017, *New Journal of Physics*, 19, 065003
- Krumholz, M. & Burkert, A. 2010, *ApJ*, 724, 895
- Krumholz, M. R. & Burkert, B. 2016, *MNRAS*, 458, 1671
- Kulsrud, R. M. 2005, *Plasma physics for astrophysics*
- Li, P. S., McKee, C. F., & Klein, R. I. 2012a, *ApJ*, 744, 73
- Li, P. S., Myers, A., & McKee, C. F. 2012b, *ApJ*, 760, 33
- Lim, J., Cho, J., & Yoon, H. 2020, *ApJ*, 893, 75
- Longcope, D. W. & Klapper, I. 1997, *ApJ*, 488, 443
- Mac Low, M.-M., Klessen, R. S., Burkert, A., & Smith, M. D. 1998, *Phys. Rev. Lett.*, 80, 2754
- Makwana, K. D. & Yan, H. 2020, *Physical Review X*, 10, 031021
- Maron, J. & Goldreich, P. 2001, *ApJ*, 554, 1175
- Matthaeus, W. H. 2021, *Physics of Plasmas*, 28, 032306
- Matthaeus, W. H., Goldstein, M. L., & Montgomery, D. C. 1983, *Phys. Rev. Lett.*, 51, 1484
- Matthaeus, W. H. & Velli, M. 2011, *Space Sci Rev*, 160, 145
- McKee, C. F. 1989, *ApJ*, 345, 782
- Monin, A. S. & l’Agglom, A. M. 1971, *Statistical fluid mechanics; mechanics of turbulence*
- Montgomery, D., Brown, M. R., & Matthaeus, W. H. 1987, *J. Geophys. Res.*, 92, 282
- Mouschovias, T. C., Ciolek, G. E., & Morton, S. A. 2011, *MNRAS*, 415, 1751
- Mouschovias, T. C., Tassis, K., & Kunz, M. W. 2006, *ApJ*, 646, 1043
- Newcomb, W. A. 1962, *Nuclear Fusion Supplement Part, 2*
- Oughton, S. & Matthaeus, W. H. 2020, *ApJ*, 897, 37
- Oughton, S., Priest, E. R., & Matthaeus, W. H. 1994, *Journal of Fluid Mechanics*, 280, 95–117
- Oughton, S., Wan, M., Servidio, S., & Matthaeus, W. H. 2013, *ApJ*, 768, 10
- Panopoulou, G., Tassis, K., Blinov, D., et al. 2015, *MNRAS*, 452, 715
- Panopoulou, G. V., Psaradaki, I., & Tassis, K. 2016, *MNRAS*, 462, 1517
- Park, J. & Ryu, D. 2019, *ApJ*, 875, 2
- Passot, T. & Vázquez-Semadeni, E. 2003, *A&A*, 398, 845
- Piontek, R. A. & Ostriker, E. C. 2007, *ApJ*, 663, 183
- Planck Collaboration, Ade, P. A. R., Aghanim, N., et al. 2016, *A&A*, 586, A138
- Schekochihin, A. A. 2020, arXiv e-prints, arXiv:2010.00699
- Schekochihin, A. A., Isakov, A. B., Cowley, S. C., et al. 2007, *New Journal of Physics*, 9, 300
- Shebalin, J. V. 2013, *Geophysical and Astrophysical Fluid Dynamics*, 107, 411
- Shebalin, J. V., Matthaeus, W. H., & Montgomery, D. 1983, *Journal of Plasma Physics*, 29, 525
- Skalidis, R., Sternberg, J., Beattie, J. R., Pavlidou, V., & Tassis, K. 2021, *A&A*, 656, A118
- Skalidis, R. & Tassis, K. 2021, *A&A*, 647, A186
- Skalidis, R., Tassis, K., Panopoulou, G. V., et al. 2022, *A&A*, 665, A77
- Sridhar, S. & Goldreich, P. 1994, *ApJ*, 432, 612
- Strauss, H. R. 1976, *Physics of Fluids*, 19, 134
- Strauss, H. R. 1977, *Physics of Fluids*, 20, 1354
- Tenerani, A. & Velli, M. 2017, *ApJ*, 843, 26
- Verdini, A. & Velli, M. 2007, *ApJ*, 662, 669
- Wan, M., Oughton, S., Servidio, S., & Matthaeus, W. H. 2012, *Journal of Fluid Mechanics*, 697, 296–315
- Yang, L., Zhang, L., He, J., et al. 2018, *The Astrophysical Journal*, 866, 41
- Yang, Y., Wan, M., Matthaeus, W. H., & Chen, S. 2021, *Journal of Fluid Mechanics*, 916, A4
- Zank, G. P., Zhao, L. L., Adhikari, L., et al. 2022, *ApJ*, 926, L16
- Zocco, A. & Schekochihin, A. A. 2011, *Physics of Plasmas*, 18, 102309
- Zweibel, E. G. & McKee, C. F. 1995, *ApJ*, 439, 779

*Acknowledgements.* We would like to thank the anonymous referee for reviewing our manuscript. We are grateful to T. Ch. Mouschovias, and P. F. Hopkins for stimulating discussions. We also thank E. N. Economou, V. Pelgrims, E. Ntormousi, A. Tsouros, and I. Komis for useful suggestions on the manuscript. This work was supported by NSF grant AST-2109127. We acknowledge support by the European Research Council under the European Union’s Horizon 2020 research and innovation programme, grant agreement No. 771282 (RS and KT); by the Hellenic Foundation for Research and Innovation under the “First Call for H.F.R.I. Research Projects to support Faculty members and Researchers and the procurement of high-cost research equipment grant”, Project 1552 CIRCE (VP); and from the Foundation of Research and Technology - Hellas Synergy Grants Program (project MagMASim, VP, and project POLAR, KT).

## Appendix A: Lagrangian of coherent cylindrical parcels

We used the MHD Lagrangian as derived by Newcomb (Newcomb 1962) for isothermal magnetized fluids. The total MHD Lagrangian is the sum of the kinetic and the total potential energy of all the fluid elements within a volume  $\mathcal{V}$ ,

$$\mathcal{L} = \int_{\mathcal{V}} \left( \frac{1}{2} \rho u^2 - P_s - \frac{B^2}{8\pi} - \frac{1}{2} \rho \Phi \right), \quad (\text{A.1})$$

where  $P_s$  is the thermal pressure, and  $\Phi$  is the gravitational potential. The equation of motion for magnetized turbulent fluids is obtained from the stationary-action principle ( $\delta \int_{t_1}^{t_2} dt \mathcal{L} = 0$ ). We focused on fluids in which magnetic pressure dominates thermal pressure ( $B^2/8\pi \gg P_s$ ), and we ignored self-gravity,  $\Phi = 0$ . Therefore, the dominant potential term in the Lagrangian is magnetic pressure. When we consider that the ensemble of the fluid elements moves as a coherent cylinder (Fig. 1), then the integration of the Lagrangian takes place within the volume of the cylinder. In this case, the integrated Lagrangian terms correspond to the kinetic and the magnetic energy of the cylinder. The perturbed Lagrangian of a cylinder is (using Eqs. 2, 3, and 4)

$$\begin{aligned} \delta \mathcal{L} = & \frac{1}{2} \rho \ell^2 \left( \frac{\delta \dot{B}_{\parallel}^2}{4B_0^2} + \frac{\delta \dot{B}_{\perp r}^2}{\delta B_{\perp r}^2} \right) + \frac{1}{2} \rho \ell_{\perp}^2 \left( \frac{\delta \dot{B}_{\perp \phi}^2}{\delta B_{\perp \phi}^2} - 2 \frac{\delta \dot{B}_{\perp r}}{\delta B_{\perp r}} \frac{\delta \dot{B}_{\perp \phi}}{\delta B_{\perp \phi}} \right) \\ & - \frac{1}{2} \rho \ell_{\parallel}^2 \frac{\delta \dot{B}_{\perp r}}{\delta B_{\perp r}} \frac{\delta \dot{B}_{\parallel}}{B_0} - \left( \frac{\delta B_{\parallel}^2}{8\pi} + \frac{\delta B_{\perp r}^2}{8\pi} + \frac{\delta B_{\perp \phi}^2}{8\pi} \right) - \frac{B_0 \delta B_{\parallel}}{4\pi}. \end{aligned} \quad (\text{A.2})$$

For untwisted cylinders, all terms containing a  $\phi$  component are zero. Then, the Lagrangian contains only the parallel and the perpendicular (longitudinal) components, which are generally coupled due to the  $\delta \dot{B}_{\perp r} \delta \dot{B}_{\parallel} / (\delta B_{\perp r} B_0) \ell_{\parallel}^2$  term. For sub-Alfvénic turbulence, this is a higher-order term because  $|B_0| \gg |\delta B|$ . By keeping the dominant (second-order) terms, we derived the total perturbed Lagrangian of a coherent cylindrical structure, which to leading order, can be expressed as the sum of two independent parts (parallel and perpendicular to the background magnetic field, Eqs. 8 and 9).

## Appendix B: Solutions of $\delta \mathcal{L}_{\parallel}$

From the Euler-Lagrange equation of  $\delta \mathcal{L}_{\parallel}$ , we obtain

$$\delta \ddot{B}_{\parallel, \ell}(t) = -(\delta B_{\parallel, \ell}(t) + B_0) \frac{4V_A^2}{\ell_{\perp, 0}^2}, \quad (\text{B.1})$$

where  $V_A = B_0 / \sqrt{4\pi\rho}$  is the Alfvénic speed.

Initially, we compressed the perturbed volume perpendicular to  $\mathbf{B}_0$ , then released it and allowed the compression to propagate. For the initial conditions, we considered that  $u_{\perp, \ell}(t=0) = 0$  and  $\delta B_{\parallel, \ell}(t=0) = \delta B_{\parallel, \max}$ . We might have initiated the fluid parcel at  $\delta B_{\parallel, \ell}(t=0) = -\delta B_{\parallel, \max}$ , but in that case,  $u_{\perp, \ell}(t=0) \neq 0$ . Solutions of Eq. B.1 are harmonic, but are valid only for early times because at later times, nonlinear interactions become important and energy is diffused. Below, we consider the scenario of energy diffusing due to the shock formation because we considered highly compressible fluids. Without loss of generality, we can consider any diffusive process.

From the jump conditions, we analytically obtained that when  $\mathcal{M}_s \gg 1$ , an isothermal shock perpendicular to  $\mathbf{B}_0$  forms when

$$\delta B_{\parallel} \lesssim \frac{B_0}{2} (\mathcal{M}_A^2 - 1). \quad (\text{B.2})$$

Thus, in sub-Alfvénic turbulence,  $\mathcal{M}_A < 1$ , magnetized shocks form when  $\delta B_{\parallel} < 0$ , which means that  $\delta B_{\parallel}$  will never perform a full harmonic cycle. Keeping the dominant term of the expansion of the harmonic solutions (Eq. B.1), we derive that

$$\delta B_{\parallel, \ell}(t) \approx \delta B_{\parallel, \max} - 2B_0 \frac{V_A^2}{\ell_{\perp, 0}^2} t^2. \quad (\text{B.3})$$

The above solution through Eq. 2 yields

$$u_{\perp, \ell}(t) \approx \frac{2V_A^2}{\ell_{\perp, 0}} t. \quad (\text{B.4})$$

From Eqs. B.3 and B.4, we obtain that as the magnetic field of the perturbed volume decreases,  $u_{\perp, \ell}$  increases. When the shock is formed, the perturbed volume instantaneously bounces off its environment, which acts as a pressure wall (Basu et al. 2009). At the post-shock phase, the motion is reversed and the coherent volume will start contracting until  $\delta B_{\parallel, \ell}$  reaches a value of  $+\delta B_{\parallel, \max, p}$ . The post-shock solutions are obtained from Eq. B.1 with initial conditions  $u_p(t=0) > 0$  and  $\delta B_{\parallel, p}(t=0) < 0$ , where the subscript  $p$  denotes post-shock quantities. At the post-shock phase, the solution of  $\delta B_{\parallel}$  is

$$\delta B_{\parallel, \ell}(t) \approx -\delta B_{\parallel, p} + u_p(t=0)t - 2B_0 \frac{V_A^2}{\ell_{\perp, 0}^2} t^2. \quad (\text{B.5})$$

At the post-shock phase, the magnetic field increases until  $+\delta B_{\parallel, \max, p}$ , which is smaller than the initial magnetic field increase ( $+\delta B_{\parallel, \max}$ ) of the pre-shock phase because energy has been dissipated by the shock (Park & Ryu 2019; Cho et al. 2022). When the perturbed volume reaches  $+\delta B_{\parallel, \max, p}$ , the velocity is zero, and the motion is reversed. Then, the volume starts expanding until it again forms a shock. Overall, the perturbed volume would perform damped oscillations until all the energy is dissipated (Basu et al. 2009; Yang et al. 2021).

Fluids in nature are commonly assumed to be constantly perturbed until turbulence reaches a steady state (Krumholz & Burkert 2010; Kritsuk et al. 2017; Colman et al. 2022). Various driving mechanisms could maintain turbulent energy in nature (Eswaran & Pope 1988; McKee 1989; Mac Low et al. 1998; Piontek & Ostriker 2007; Elmegreen 2009; Krumholz & Burkert 2016; Girichidis et al. 2016; Hanasoge et al. 2020; Iffrig, Olivier & Hennebelle, Patrick 2017; Klessen & Hennebelle 2010; Elmegreen & Scalo 2004). In our model, turbulent driving is equivalent to adding externally kinetic energy to the perturbed volume, such that the initial velocity at the post-shock phase,  $u_p(t=0)$ , is sufficient to compress the perturbed volume until it reaches the maximum compression it had in the pre-shock phase,  $\delta B_{\parallel, \max, p} \approx +\delta B_{\parallel, \max}$ .

We considered an external driver, which ensured that  $\delta B_{\parallel}$  fluctuations, and hence energy, were maintained in a quasi-static state. In addition, we considered that the fluid is ergodic (Monin & I'Agglom 1971; Galanti & Tsinober 2004). For ergodic fluids,  $\delta B_{\parallel, \ell}$  are characterized by ballistic profiles,  $\delta B_{\parallel, \ell} \propto t^2$ , and as we argue below, they bounce between  $+\delta B_{\parallel, \max}$  and  $-\delta B_{\parallel, \max}$  within a characteristic timescale  $\mathcal{T}_{\perp} \approx 4\ell_{\perp, 0} V_A^{-1} \sqrt{\delta B_{\parallel, \max} / 2B_0}$ .

When we initially compressed the magnetic field of the perturbed volume along  $\mathbf{B}_0$ , then  $\ell_\perp$  decreased due to Eq. 5. This forced the surface of the environment of the perturbed volume to increase by equal amounts. Thus, the  $+\delta B_{\parallel,\max}$  initial increase of the magnetic field of the perturbed volume causes the magnetic field of the environment to decrease by  $-\delta B_{\parallel,\max}$  due to flux freezing. If the fluid is ergodic, then different fluid parcels correspond to different oscillation phases of the target fluid parcel (Monin & I'Agglom 1971; Galanti & Tsinober 2004). Therefore, the  $-\delta B_{\parallel,\max}$  of the environment corresponds to the maximum decrease in magnetic field strength of the target volume. Nonlinear effects can break the symmetry between  $+\delta B_{\parallel,\max}$  and  $-\delta B_{\parallel,\max}$ , but ergodicity is only weakly broken when  $\mathbf{B}_0 \neq 0$  (Shebalin 2013).

The perturbed volume would spend most of its time in the compressed state because the velocity is minimum there. On the other hand, the velocity of the fluid parcel is maximum when  $\delta B_{\parallel,\ell} < 0$ , and hence the fluid parcel would spend minimum time there. As a result, the majority of fluid parcels at a given time would be compressed ( $\delta B_{\parallel,\ell} > 0$ ) due to ergodicity, which is verified by numerical simulations (Beattie et al. 2022b).

### Appendix C: Solutions of $\delta\mathcal{L}_\perp$

From the Euler-Lagrange equation of  $\delta\mathcal{L}_\perp$ , we obtain

$$\delta\ddot{B}_{\perp,\ell}(t)\delta B_{\perp,\ell}(t) - 2\delta\dot{B}_{\perp,\ell}^2(t) + \frac{\delta B_{\perp,\ell}^6(t)}{4\pi\rho C^2} = 0. \quad (\text{C.1})$$

For  $|\mathbf{B}_0| \gg |\delta\mathbf{B}|$ , the sixth-order term above can be neglected, and then the solutions are straightforward. The total pressure of the fluid exerted by  $\delta B_\perp$  is transferred to parallel motions (Eq. 3), hence  $\rho u_{\parallel,\max}^2/2 = \delta B_{\perp,\max}^2/(8\pi)$ . We derive the following solutions:

$$\delta B_{\perp,\ell}(t) \approx \frac{fB_0}{1 \pm t/\mathcal{T}_\parallel}, \quad u_{\parallel,\ell}(t) \approx \pm fV_A, \quad (\text{C.2})$$

where  $\ell_\parallel(t=0) = \ell_{\parallel,0}$ ,  $f = \delta B_{\perp,\max}/B_0 \ll 1$ , and  $\mathcal{T}_\parallel = fV_A^{-1}\ell_{\parallel,0}$ . In the above equations, the signs depend on the initial conditions. Initially, we considered that  $\delta B_{\perp,\ell}(t=0) = \delta B_{\perp,\max}$ , and  $u_{\parallel,\ell}(t=0) = u_{\perp,\max}$ , which leads to positive signs.

If the initial velocity along  $\mathbf{B}_0$  were zero, then both  $u_{\parallel,\ell}$  and  $\delta B_{\perp,\ell}$  would remain static. The coupling of parallel and perpendicular motions (Eq. 3) would induce parallel motions when  $\delta\dot{B}_{\parallel,\ell} \neq 0$ , even if  $u_{\parallel,\ell}(0) = 0$ . However, because we have neglected the coupling of motions, we initiated  $u_{\parallel,\ell}$  from the initial conditions.

From Eq. 6, we obtain that the free streaming of the perturbed volume causes  $\ell_\parallel$  to expand or contract as

$$\ell_\parallel(t) \approx \ell_{\parallel,0} \left( 1 \pm \frac{t}{\mathcal{T}_\parallel} \right). \quad (\text{C.3})$$

As the target fluid parcel expands, its environment along the  $\mathbf{B}_0$  axis contracts, provided that the fluid has fixed boundaries. Due to the expansion of the target volume, the initial velocity of the environment would be  $-u_{\parallel,\max}$ , which causes a negative sign in the denominator of Eq. C.2, and hence  $\delta B_{\perp,\ell}$  increases in the environment. On the other hand,  $\delta B_{\perp,\ell}$  in the target volume stops increasing when  $t = \mathcal{T}_\parallel$  because  $\delta B_{\perp,\ell}$  in the environment becomes infinite. In sub-Alfvénic flows,  $|\mathbf{B}_0| \gg |\delta\mathbf{B}_\perp|$ , so that this infinity should be treated as an asymptotic behaviour of  $\delta B_{\perp,\ell}$ : there is a physical limit above which  $\delta B_{\perp,\ell}$  cannot grow. After

$\mathcal{T}_\parallel$ , the motion is reversed and the environment starts expanding along  $\mathbf{B}_0$ , causing the target volume to contract with  $\delta B_{\perp,\ell}$  growing as  $\delta B_{\perp,\ell}(t) \approx fB_0/(2 - fV_A\ell_{\parallel,0}^{-1}t)$  until it reaches  $\delta B_{\perp,\max}$ .

<sup>2</sup> This solution is obtained by considering that the initial conditions in the reversed motion of the fluid parcel are  $\delta B_{\perp,\ell}(0) = \delta B_{\perp,\max}/2$ ,  $u_{\parallel,\ell}(0) = -u_{\parallel,\max}$ , and  $\ell_\parallel(0) = 2\ell_{\parallel,0}$ . These values correspond to the solutions of Eqs. C.2 and C.3 for  $t = T_\parallel$ .